SCIENTIFIC REPORTS

OPEN

SUBJECT AREAS:
FLUID DYNAMICS
CHEMICAL ENGINEERING
IMAGING AND SENSING

Received
28 January 2014

Accepted
7 May 2014

Published
28 May 2014

Correspondence and requests for materials should be addressed to J.H.J. (jhje@postech.ac.kr)

Four-dimensional visualization of rising microbubbles

Ji Won Jung[1], Hyung Min Jeon[1], Jaeyeon Pyo[1], Jae-Hong Lim[2], Byung Mook Weon[3], Yoshiki Kohmura[4], Tetsuya Ishikawa[4] & Jung Ho Je[1,4]

[1]X-ray Imaging Center, Department of Materials Science and Engineering, Pohang University of Science and Technology, San 31, Hyoja-dong, Pohang 790-784, Korea, [2]Pohang Accelerator Laboratory, San 31, Hyoja-dong, Pohang 790-784, Korea, [3]School of Advanced Materials Science and Engineering, SKKU Advanced Institute of Nanotechnology (SAINT), Sungkyunkwan University, Suwon 440-746, Korea, [4]RIKEN/SPring-8, 1-1-1 Kouto, Mikazuki-cho, Sayo-gun, Hyogo 679-5148, Japan.

Four-dimensional imaging, which indicates imaging in three spatial dimensions as a function of time, provides useful evidence to investigate the interactions of rising bubbles. However, this has been largely unexplored for microbubbles, mostly due to problems associated with strong light scattering and shallow depth of field in optical imaging. Here, tracking x-ray microtomography is used to visualize rising microbubbles in four dimensions. Bubbles are tracked by moving the cell to account for their rise velocity. The sizes, shapes, time-dependent positions, and velocities of individual rising microbubbles are clearly identified, despite substantial overlaps between bubbles in the field of view. Our tracking x-ray microtomography affords opportunities for understanding bubble-bubble (or particle) interactions at microscales – important in various fields such as microfluidics, biomechanics, and floatation.

The rising of bubbles, induced by buoyancy, commonly occurs in natural and industrial processes. Understanding the interactions between rising bubbles is important not only for scientific interests but also for industrial applications. Many theoretical[1–3], numerical[4–8], and experimental[9–14] investigations have been performed on bubble interactions over several decades.

Four-dimensional (4-D) imaging (3 spatial dimensions + time) of rising bubbles allows us to directly measure their sizes, shapes, time-dependent positions and velocities. These are key parameters in bubble interactions. Recently, 4-D imaging of rising bubbles has been developed, in particular, for large bubbles (>1 mm) in a high Reynolds number regime, based on optical tomography[15–17] or magnetic resonance imaging[14]. However, 4-D imaging of microbubbles ($\ll 1$ mm) in low Reynolds-number flows has not yet been achieved, despite the importance of microbubbles in many processes such as microfluidics[18–20], biomechanics of microorganisms[21–23], the dynamics of lava flow[24,25], and bubble-particle interactions in flotation cells. This is because of difficulties associated with strong light scattering and shallow depth of field in optical imaging that occurs, in particular, in high resolution imaging.

Phase contrast x-ray imaging[26–29] provides excellent contrasts in microbubble boundaries of gas−liquid systems[30–34]. Fast x-ray microtomography using phase contrast x-ray imaging has been also developed for 4-D visualization of quasi-static microbubbles[28,29]. Here, we introduce the development of a tracking x-ray microtomography that visualizes rising microbubbles in 4-D by counterbalancing their rise. Even in the presence of substantial overlap between imaged bubbles, the sizes, shapes, time-dependent positions and velocities of individual rising microbubbles can be accurately measured.

Results

The experimental setup of the tracking x-ray microtomography is schematically illustrated in Fig. 1(a). The experiments were performed at the BL29XU RIKEN beamline[29] of SPring-8 and at the 6D X-ray Micro-Imaging beamline of PLS-II. This is different from the fast x-ray microtomography reported previously[29]; the key idea of this setup is to track rising microbubbles, specifically by accounting for their rise by moving down an in-situ cell (IC) at the same speed as the rising bubbles [Fig. 1(b)].

Figure 1(c) shows representative equi-angular series of projection images for three unequal-sized microbubbles, taken with the tracking x-ray microtomography during their rise in a pure glycerol[30]. Microradiographs were taken per an equi-angular series of projection images. The time interval between consecutive equi-angular series was 2.5 s. Strikingly, boundaries of individual microbubbles could be clearly resolved with the aid of x-ray phase

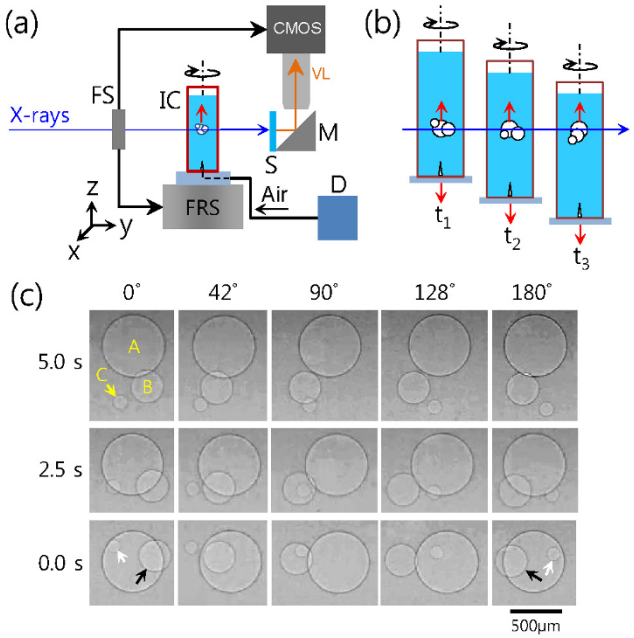

Figure 1 | Schematic illustration of 4-D visualization. (a) Schematic of tracking x-ray microtomography for 4-D visualization of rising microbubbles. (b) Conceptual schematic of counterbalancing the rise of microbubbles: an in-situ cell is moving down with the same speed as their rise. (c) Representative equi-angular series of projection images for three of unequal-size microbubbles during their rise in pure glycerol.

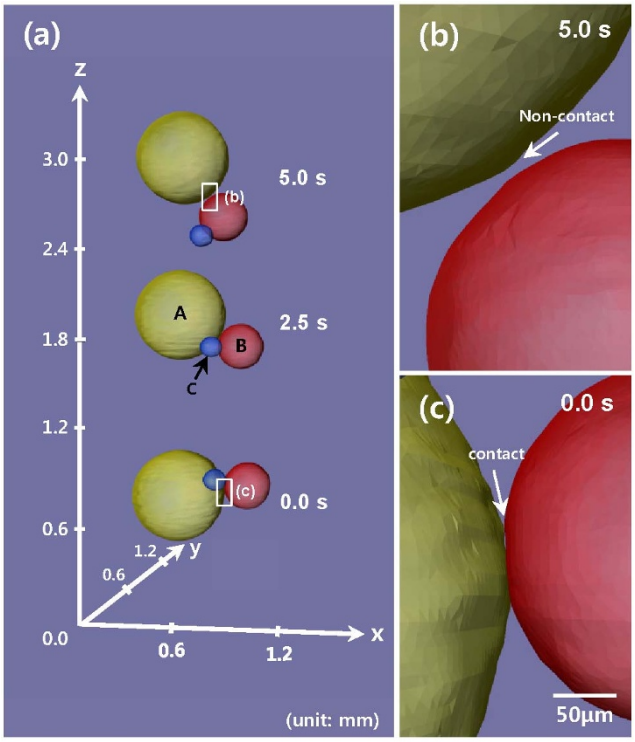

Figure 2 | Successful illustration of rising microbubbles. (a) Reconstructed 4-D image of the rising microbubbles shown in Fig. 1(c) and close-up views of the bubbles at (b) t = 5.0 s and (c) t = 0.0 s (white boxes in Fig. 2(a)). The contact (c) or non-contact (b) of two microbubbles was clearly observable.

contrast edge enhancement, even with horizontal overlap between bubbles. The sizes and shapes of the bubbles (A, B, and C) were clearly identified despite their rise at ~100 μm/s, a relatively high speed comparing to the effective pixel size of the CMOS camera (4.0 μm). The sizes of bubbles A, B, and C were measured to be 580, 300, and 120 μm in diameter, respectively. There was no noticeable change in the bubble shapes during their rise, as demonstrated by their circular shapes in each angle and time. Here, the time was set to be zero for the acquisition of the first angular data set.

The counterbalance was performed to account for the rising speed of a bubble cluster, instead of each bubble. In reality, the z-coordinate of a bubble in each projection image showed a slight variation in a given equi-angular set of projections because of slight differences in the rising speeds of individual bubbles (see, for instance, the bubble B (C) marked by the black (the white) arrows in 0° and 180° at 0.0 s in Fig. 1(c)). Therefore, for proper reconstruction all the images in the angular set were shifted using an image shift function to match the z-coordinate in each projection image to a reference value, i.e. the z-coordinate at 0°. Such an image shift process was repeated for each bubble and for each angular set. Tomographic reconstruction was then carried out using Octopus® (Ghent University, Germany), a commercial tomographic reconstruction software based on a filtered-back projection algorithm. Volume rendering of reconstructed images was performed with AMIRA® (MercuryTM Computer Systems Inc., USA).

Figure 2(a) shows a reconstructed 4-D image of the rising microbubbles in Fig. 1(c). Time-dependent 3-D configurations of the three rising bubbles were visualized; hence we were able to vividly demonstrate how a bigger bubble passes by a smaller bubble. Importantly, this technique accurately extracts the positions of the three bubbles and their dynamics (see supplementary Table 1). Furthermore, the contact or non-contact between two microbubbles can be clearly identified (Figs. 2(b), (c), and supplementary Movie 1). This is particularly important in understanding bubble interactions.

Discussion

One big advantage of our tracking x-ray microtomography technique is its capability to visualize rising microbubbles with substantial horizontal overlap in real-time in 3-D geometry. We tested a cluster with six, unequal-sized microbubbles. Despite a substantial overlap along the main axis of the cluster (see the inset in the left-top corner in Fig. 3), we were able to visualize individual microbubbles in 3-D at 0.0 s (see supplementary Movie 2). Remarkably, a very small microbubble of 15 μm (white arrow) that was located between big bubbles could be clearly reconstructed in 3-D – something which is not possible using conventional 3-D imaging methods.

Additionally, the spatial and temporal configurations of the rising microbubbles were clearly identified, as demonstrated by the reconstructed 4-D images at 0.0 and 28.0 s (side view – Fig. S1(a), top view – Fig. S1(b)). We observed that the bubbles were slightly aligning horizontally (see the white arrows in Fig. S1(a)) but spreading in the x- or y-direction, as specifically demonstrated by the time-dependent standard deviations of their positions in Figs. S1(c) and S1(d), respectively. Note that with this new technique we can record very small changes in standard deviation, for instance $|\Delta\sigma| < 4$ μm for 28 s in the z-axis (Fig. S2) or in the x- or y-axis (Fig. S2).

We finally tested time-dependent behaviors of a microbubble cluster of different sized bubbles (Fig. 4). The reconstructed 3-D images in Fig. 4(a) demonstrate a dynamic sequence of non-contact (0.0 s), contact (15.0 to 32.5 s), and coalescence (35.0 s) of bubble B and bubble A, and show a faster rise of the coalesced bubble A′ than bubble C (60.0 s) (see supplementary movie 3). In contrast with the rising speed of in-line equal-sized bubbles[35], that of microbubbles showed a tendency to decrease before the coalescence (Fig. 4(b)), presumably associated with the existence of a small bubble (B) in-between. By the coalescence, interestingly, there was a jump in the rising speed of bubble A′ or C. The speed then increased with higher acceleration in bubble A′ than in bubble C. Furthermore, our 4-D

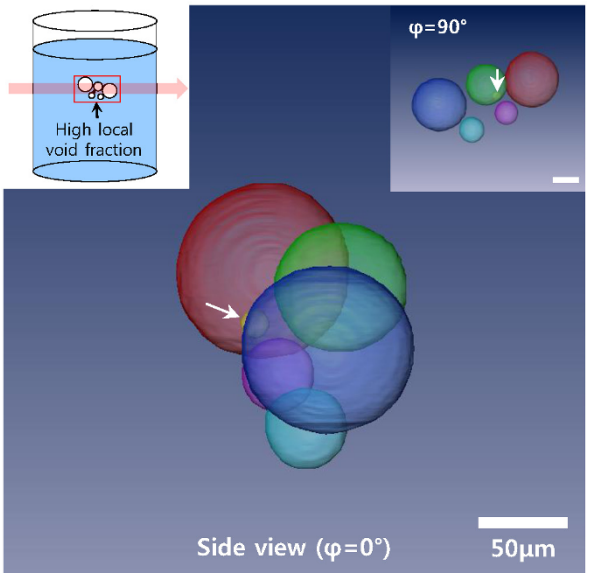

Figure 3 | Geometric analysis of rising microbubbles. Side view of a reconstructed bubble cluster with six microbubbles. The sizes and 3-D positions of six bubbles are clearly identified despite substantial horizontal overlaps between the bubbles, as illustrated in the inset on left-top corner. (Inset on right-top corner: side view at φ = 90°, scanning time for 60 projections: 1.0 s, effective pixel size: 1.0 μm).

visualization allowed us to accurately determine relative configurations such as the inclination angle θ, the non-dimensional distance S (=d/R_C, implying d = the distance between bubbles A and C, R_C = the radius of bubble C), and the azimuthal angle φ between bubble A (A′) and bubble C, illustrated in Fig. 4(a) at 32.5 s and the inset of Fig. 4(d). In Fig. 4(c), θ (blue solid circles) showed opposite behaviors before and after the coalescence and a discontinuity, similar to the singularity of the rising speed, in the coalescence. The distance S [black solid triangles in Fig. 4(c)] showed a downward hump right after the coalescence, possibly due to capillary waves carrying momentum[34]. Meanwhile, the azimuthal angle $\varphi_{A(A')\text{-}C}$ showed a large variation over the rising time (Fig. 4(d)).

In summary, we have developed a tracking x-ray microtomography for 4-D imaging of rising microbubbles by counterbalancing their rise. The sizes, shapes, and time-dependent positions and velocities of microbubbles (<500 μm) were clearly identified in 3-D, despite their rise and horizontal overlap between the bubbles. The results in this study efficiently demonstrate the capability of the tracking x-ray microtomography to visualize and accurately quantify configurations of microbubbles. This currently cannot be achieved with any other 4-D imaging methods at such a high spatial resolution. We believe that the tracking x-ray microtomography is a powerful tool that can reveal key physics that underlies the interactions of moving microbubbles or particles in a low Reynolds or a Stokes flow regime – important in various fields such as microfluidics, biomechanics, and floatation[36,37]. Generally speaking, 4-D visualization for soft matter or biomedical samples with the x-ray microtomography[38,39] provides a powerful tool with great versatility.

Methods

The experiments were performed at the BL29XU RIKEN beamline[29] (E = 4.4 ~ 37.8 keV, ΔE/E ~ 1.3 × 10^{-4}) of SPring-8 and at the 6D X-ray Micro-Imaging beamline (E_c = 9.0 keV, ΔE/E ~ 1.0) of PLS-II with the experimental setup as schematically illustrated in Fig. 1(a). Unlike the fast x-ray microtomography reported previously[29], the key idea of this setup is to track rising microbubbles, specifically by accounting for their rise by moving down an in-situ cell (IC) at the same speed as the rising bubbles (Fig. 1b). In detail, the in-situ cell, while rotated at 30 or 60 rpm around the z-axis, was translated in the minus z-direction with the premeasured rising speed of a microbubble cluster during the tomographic experiments, allowing the x-ray beam to always pass through the rising bubble cluster. The in-situ cell, a Kapton tube (10 mm-diameter with 100 μm wall thickness) on an aluminum base with a microneedle (tip radius: 1 μm), filled with a liquid medium, was mounted on a fast rotary stage (AEROTECH ABRS-150MP). Microbubbles were generated from the microneedle by applying air pulses (10 ~ 100 psi air pressure, 30 ~ 500 ms) from an air dispenser (D, Nordson EFD UltimusTM-I). Here, the centrifugal force on a bubble due to the rotation of the in-situ cell (30 or 60 rpm) was negligible (smaller than 0.1% of the gravitational force). After passing through the in-situ cell, the transmitted x-rays were converted by a scintillator (S) to visible lights (VL), which were then reflected by a mirror (M) and magnified by an objective lens (Mitutoyo M Plan Apo 5, NA = 0.14). After magnification, the image on the scintillator was captured by a CMOS camera (1,024 × 1,024 pixels; Photron SA 1.1, Photron) that was synchronized with the fast rotary stage (FRS) and a fast shutter (FS). The whole imaging system was carefully aligned to gravity by using a digital inclinometer with 0.001° accuracy.

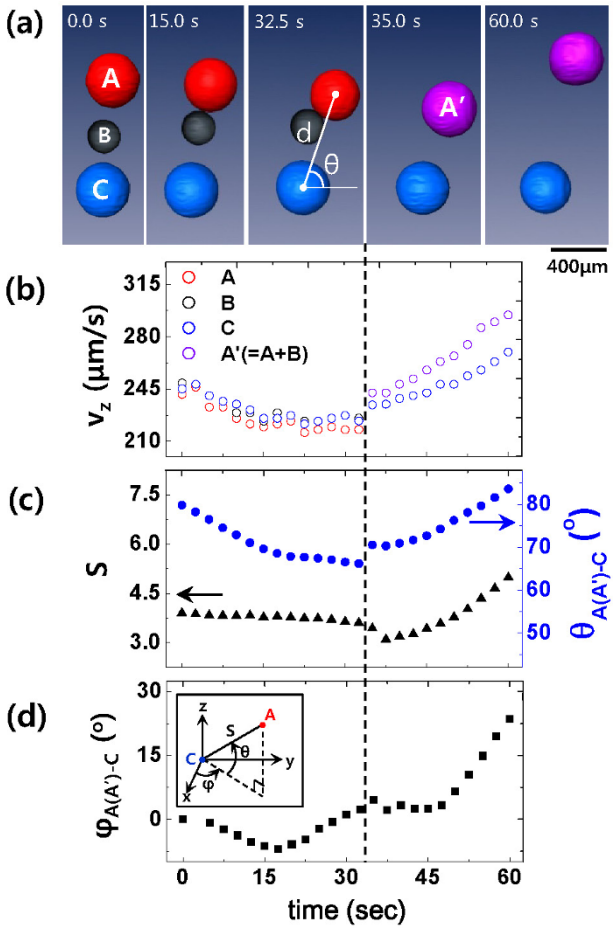

Figure 4 | Dynamics of a rising microbubble cluster. (a) Reconstructed 3-D images of a rising microbubble cluster, demonstrating a dynamic sequence of non-contact (0.0 s), contact (15.0 to 32.5 s), coalescence (35.0 s) of bubble B and bubble A, and showing a faster rise of the coalesced bubble A' than bubble C (60.0 s). (b) Rising speeds of microbubbles, (c) non-dimensional distance (S = d/R) and inclination angle (θ), and (d) azimuthal angle (φ) between leading (A) and trailing (C) bubbles, as a function of rising time. Scale bar: 200 μm.

1. van Wijngaarden, L. & Jeffrey, D. J. Hydrodynamic interaction between gas bubbles in liquid. *J. Fluid Mech.* **77**, 27–44 (1976).
2. van Wijngaarden, L. The mean rise velocity of pairwise-interacting bubbles in liquid. *J. Fluid Mech.* **251**, 55–78 (1993).
3. Kok, J. B. W. Dynamics of a pair of gas bubbles moving through liquid. Part I. Theory. *Eur. J. Mech. B: Fluids* **12**, 515–540 (1993).
4. Smereka, P. On the motion of bubbles in a periodic box. *J. Fluid Mech.* **254**, 79–112 (1993).
5. Sangani, A. S. & Didwania, A. K. Dynamic simulations of flows of bubbly liquids at large Reynols numbers. *J. Fluid Mech.* **250**, 307–337 (1993).
6. Legendre, D., Magnaudet, J. & Mougin, G. Hydrodynamic interactions between two spherical rising side by side in a viscous liquid. *J. Fluid Mech.* **497**, 133–166 (2003).

7. Dijkhuizen, W., Roghair, I., Annaland, M. V. & Kuipers, J. A. M. DNS of gas bubbles behavior using an improved 3D front tracking model-Drag force on isolated bubbles and comparison with experiments. *Chem. Eng. Sci.* **65**, 1415–1426 (2010).
8. Hallez, Y. & Legendre, D. Interaction between two spherical bubbles rising in a viscous liquid. *J. Fluid Mech.* **673**, 406–431 (2011).
9. Cartellier, A. & Rivière, N. Bubble-induced agitation and microstructure in uniform bubbly flows at small to moderate particle Reynolds numbers. *Phys. Fluids* **13**, 2165–2181 (2001).
10. Zenit, R., Koch, D. L. & Sangani, A. S. Measurements of the average properties of a suspension of bubbles rising in a vertical channel. *J. Fluid Mech.* **429**, 307–342 (2001).
11. Risso, F. & Ellingsen, K. Velocity fluctuations in a homogeneous dilute dispersion of high-Reynolds-number rising bubbles. *J. Fluid Mech.* **453**, 395–410 (2002).
12. Sanada, T., Sato, A., Shirota, M. & Watanabe, M. Motion and coalescence of a pair of bubbles rising side by side. *Chem. Eng. Sci.* **64**, 2659–2671 (2009).
13. Mercado, J. M. *et al*. On bubble clustering and energy spectra in pseudoturbulence. *J. Fluid Mech.* **650**, 287–306 (2010).
14. Tayler, A. B., Holland, D. J., Sederman, A. J. & Gladden, L. F. Exploring the origins of turbulence in multiphase flow using compressed sensing MRI. *Phys. Rev. Lett.* **108**, 264505 (2012).
15. Chaouki, J., Larachi, F. & Dudukovic, M. P. Noninvasive tomographic and velocimetric monitoring of multiphase flows. *Ind. Eng. Chem. Res.* **36**, 4476–4503 (1997).
16. Rzasa, M. R. & Plaskowski, A. Application of optical tomography for measurements of aeration parameters in large water tanks. *Meas. Sci. Technol.* **14**, 199–204 (2003).
17. Pokusaev, B. G., Kazenin, D. A. & Karlov, S. P. Immersion tomographic study of the motion of bubbles in a flooded granular bed. *Theor. Found. Chem. Eng.* **38**, 561–568 (2004).
18. Marmottant, P. & Hilgenfeldt, S. A bubble-driven microfluidic transport element for bioengineering. *Proc. Natl. Acad. Sci. U. S. A.* **101**, 9523–9527 (2004).
19. Marmottant, P. *et al*. Microfluidics with ultrasound-driven bubbles. *J. Fluid Mech.* **568**, 109–118 (2006).
20. Jensen, M. J., Stone, H. A. & Bruus, H. A numerical study of two-phase Stokes flow in an axisymmetric flow-focusing device. *Phys. Fluids* **18**, 077103 (2006).
21. Purcell, E. M. Life at low Reynolds number. *Am. J. Phys.* **45**, 3–11 (1977).
22. Lauga, E. & Powers, T. R. The hydrodynamics of swimming microorganisms. *Rep. Prog. Phys.* **72**, 096601 (2009).
23. Lin, Z., Thiffeault, J.-L. & Childress, S. Stirring by squirmers. *J. Fluid Mech.* **669**, 167–177 (2011).
24. Manga, M. & Stone, H. A. Interactions between bubbles in magmas and lavas: effects of bubble deformation. *J. Volcanol. Geotherm. Res.* **63**, 267–279 (1994).
25. Okumura, S. *et al*. Experimental constraints on permeable gas transport in crystalline silicic magmas. *Contrib. Mineral. Petrol.* **164**, 493–504 (2012).
26. Wilkins, S. W. *et al*. Phase-contrast imaging using polychromatic hard X-rays. *Nature* **384**, 335–338 (1996).
27. Margaritondo, G., Hwu, Y. & Je, J. H. Synchrotron light in medical and materials science radiology. *Riv. Nuovo Cimento* **27**, 1–40 (2004).
28. Mokso, F. M. R. & Stampanoni, M. Real time tomography at the Swiss Light Source. *AIP Conf. Proc.* **1234**, 87–90 (2010).
29. Jung, J. W. *et al*. Fast microtomography using bright monochromatic x-rays. *Rev. Sci. Instrum.* **83**, 093704 (2012).
30. Weon, B. M., Je, J. H., Hwu, Y. & Margaritondo, G. A coherent synchrotron X-ray microradiology investigation of bubble and droplet coalescence. *J. Synchrotron Radiat.* **15**, 660–662 (2008).
31. Lee, J. S. *et al*. Size limits the formation of liquid jets during bubble bursting. *Nat. Commun.* **2**, 367 (2011).
32. Lee, J. S., Weon, B. M., Je, J. H. & Fezzaa, K. How does an air film evolve into a bubble during drop impact? *Phys. Rev. Lett.* **109**, 204501 (2012).
33. Weon, B. M. *et al*. Colloidal wettability probed with X-ray microscopy. *Curr. Opin. Colloid Interf. Sci.* **17**, 388–395 (2012).
34. Weon, B. M. & Je, J. H. Coalescence preference depends on size inequality. *Phys. Rev. Lett.* **108**, 224501 (2012).
35. Happel, J. & Brenner, H. *Low Reynolds Number Hydrodynamics* (Kluwer, Boston, 1983).
36. Miettinen, T., Ralston, J. & Fornasiero, D. The limits of fine particle flotation. *Miner. Eng.* **23**, 420–437 (2010).
37. Liu, S. *et al*. Effect of micro-bubbles on coagulation flotation process of dyeing wastewater. *Sep. Purif. Technol.* **71**, 337–346 (2010).
38. Chang, S. *et al*. Tracking X-ray microscopy for alveolar dynamics in live intact mice. *Sci. Rep.* **3**, 1304 (2013).
39. Bech, M. *et al*. In-vivo dark-field and phase-contrast x-ray imaging. *Sci. Rep.* **3**, 3209 (2013).

Acknowledgments

Authors thank Dr. Sunghwan Jung for helpful discussions, Mr. Hyo-yun Kim for his instrumental assistance at the beamline 6D of PLS-II, and Dr. Robert Style for his kind help for the final editing. This work was supported by the National Research Foundation of Korea (NRF) grant funded by the Korea government (MSIP) (2006-0050683) and by Brain Korea 21 PLUS project for Center for Creative Industrial Materials.

Author contributions

J.W.J. designed and performed experiments and analyzed data. H.M.J. and J.P. assisted in experiments. J.H.L. helped to run synchrotron X-ray imaging experiments in PLS-II. Y.K. and T.I. helped to run synchrotron X-ray imaging experiments in SPring-8. B.M.W. helped to design experiments and interpret data. J.H.J. supervised project and helped to design experiments. J.W.J. and J.H.J. wrote the initial manuscript and B.M.W. edited the final version. All authors reviewed the final manuscript.

Additional information

Supplementary information accompanies this paper at http://www.nature.com/scientificreports

Competing financial interests: The authors declare no competing financial interests.

How to cite this article: Jung, J.W. *et al*. Four-dimensional visualization of rising microbubbles. *Sci. Rep.* **4**, 5083; DOI:10.1038/srep05083 (2014).